Optimum gaits of 2D thunniform locomotion for efficient swimming and performance of fish pair

YiQin Xu* and Yulia Peet†
School for Engineering of Matter, Transport and Energy, Arizona State University

The goal of this paper is to determine the optimum modes of aquatic locomotion for a tuna-like thunniform swimmer under water, and study the performance of paired thunniform swimmers. The computational framework is developed that couples a high-order fully-resolved numerical simulation of self-propelling flexible thunniform swimmer with the gradient-free optimization procedure based on evolutionary algorithm. The optimization is performed to find the optimum kinematic gaits of a single swimmer which are cost-efficient in start-up propulsion or maintaining constant speed. The performance of a fish pair is investigated under a selected swimming mode with various lateral separation distance under in-phase and anti-phase configuration.

I. Introduction

Understanding the mechanisms of bio-inspired aquatic locomotion is crucial for design and control of autonomous engineered systems capable of performing various scientific and defense-related missions, such as oceanic observation, data gathering, hull inspection, surveillance and combat support. Energy consumption, as well as efficiency then play an important role in robot fish design.

In nature , among the fish locomotion, thunniform group contains high-speed and long-distance swimmers such as tunas and lamnid sharks. By bio-inspiration, many researchers try to build various robot fish based on thunniform swimmers such as soft-robot thunniform fish [1, 2]. Their work was able to overcome many difficulties in designing a fish-like robot while the optimized allowable swimming mode is still unknown. Although the swimming motion for the robot in reality has many constraints due to the design of engineered system or the mechanisms itself, but it is still captivating to figure out the theoretical idealized swimming motion under certain physical constraints. To achieve the goal of optimizing the swimming efficiency of a start-up propulsion or maintaining a high-speed steady-state swimming for a single fish, a Covariance Matrix Adaptation Evolution Strategy (CMA-ES) optimization approach [3] is used to search for the ideal swimming modes.

For collective operations in robotic swarms, it is important to know the mechanisms of interaction between the agents, and how these interactions influence the overall efficiency of a swarm. In particular, for the underwater propulsion, the life aquatic animals are known to organize themselves into specific swimming patterns within a larger collective unit, a school or a shoal [4–6]. The question of what determines these specific patterns in a fish school has been intriguing the researchers for years, with no obvious answer yet apparent.

The early studies have attributed the motives of biological self-organization in fish schools to purely social functions, such as foraging [7], defense from predators [8, 9], and mating [6]. First mathematical attempts to model collective behavior in fish schools appeared in early eighties in which the interaction rules between the agents were based on entirely behavioral principles, i.e. the rules of repulsion, attraction and alignment with the neighbors [10–12]. While these models were able to reproduce a general geometrical shape of fish schools [13, 14], many questions remained unanswered, for example related to the difference in preferred patterns among fishes swimming with different velocities, larvae versus adult fish, and different fish species [15, 16].

Furthermore, an evidence has been emerging of the importance of hydrodynamic effects in the principles of schooling, such as energetics and efficiency of swimming [4, 17, 18]. Attempts to incorporate potential-flow type approaches to include hydrodynamic effects into the collective swimming models have appeared [19, 20]. The potential flow models are still far from being a realistic approximation of the fluid environment in which fishes interact, furthermore, they neglect important effects related to the fluid viscosity, fish morphology, kinematics and inertia. Fully-resolved Computational Fluid Dynamics (CFD) simulations based on the solution of the Navier-Stokes equations are capable of accounting for these effects. A number of researchers have recently used this approach to study the mechanisms

*Ph.D. student, AIAA member, e-mail: yiqinxu@asu.edu
†Assistant Professor, AIAA member, e-mail: ypeet@asu.edu

of biolocomotion and the fluid-body interactions in relation to a single fish swimming [21–23]. Several optimization studies for single anguilliform swimmers can also be acknowledged [24–26], while optimization studies for the multiple swimmers and their extension to a thunniform motion are not yet available, to the authors knowledge.

The current paper aims to fill the gap in knowledge of identifying the optimum kinematic gaits for a single thunniform fish under water environment as well as the optimum fish-pair configurations, including the effects of the vortex-wake interactions, synchronization, and the separation distance on the mechanisms of paired swimmers.

II. Modeling Framework

A. Geometrical and Kinematic Model of Thunniform Fish

The geometry of a two-dimensional thunniform fish is modeled according to the top view cross-section of a three-dimensional thunniform fish from [1, 2] as

$$y(x) = r_1 \sin(r_2 x) + r_3 \sin(r_4 x), \tag{1}$$

where $r_1 = 0.055l$, $r_2 = \frac{2\pi}{1.25l}$, $r_3 = 0.08l$, and $r_4 = \frac{2}{l}$. The function above describes the geometry of the whole body length apart from the tail, so the length l in Eq. (1) corresponds to the total body length minus the length of the tail. x coordinate is in the swimming forward direction while y is in the lateral direction. Eq. (1) corresponds to the upper curve of the body, $y_u(x)$, while the equation for the lower curve of the body would be simply $y_l(x) = -y_u(x)$, since the geometry is symmetric around its middle line. The total dimensional length L of the fish (including the tail) is chosen from a realistic soft robotic tuna [1] to be 0.3 m. To model a sharp tail, an extended length is implemented linearly from 0.25 m to 0.3 m, and thus l is 0.25 m in Eq. (1). The original static shape of the thunniform fish model is presented in Fig. 1(a).

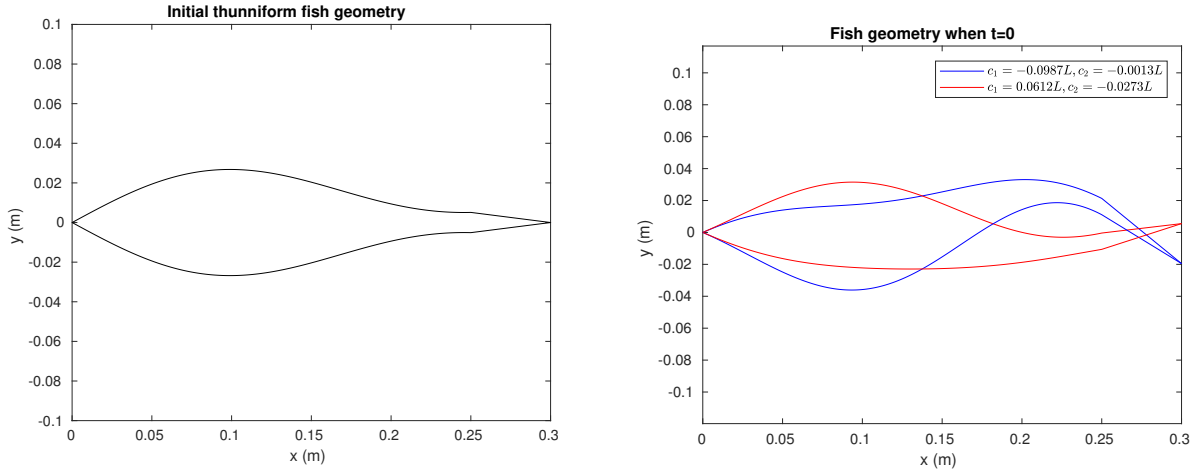

(a) Static fish geometry.

(b) Initial position at $t = 0$.

Fig. 1 Geometrical model of the fish.

The typical lateral body locomotion with negligible head motion (recoil) [1, 2, 27, 28] of a fish is described by its middle line position as

$$y_m(x,t) = [c_1 \frac{x}{L} + c_2 (\frac{x}{L})^2] \sin(2\pi(\frac{x}{\lambda L} - ft)), \tag{2}$$

where c_1 and c_2 are dimensional undetermined linear and quadratic wave amplitude envelope, λ is the body wave length which is 1.1 for a thunniform fish suggested in [1] and f is the body wave tail-beat frequency. Although the tail-beat frequency has a potential positive correlation with the swimming speed and propulsion efficiency, here we have chosen to constraint f to be equal to 1 Hz. When the middle line of a fish body moves, the upper and lower part of the body are considered to move with the same velocity in lateral direction only. Thus thrust would be purely passive since the undulatory work is done in its orthogonal direction which has zero contribution to a forward motion. A family of possible swimming modes of a thunniform fish in this paper are then described by $\{c_1, c_2\}$. One may also notice that the

initial position of the middle line from Eq. (2) is not the same as the original static geometry presented in Fig. 1, nor it represents an actual fish position at any time of motion. Thus a virtual ramp is set up before the start of the simulation to move the geometry to its starting position.

For a fish pair simulation, the geometry and the kinematic description are the same as for the single fish simulation. A second fish is placed to swim adjacent to the first fish in the lateral direction, so that they swim in parallel with their heads lined up. In the current paper, we consider their paired motion configuration as being either in-phase or in anti-phase, with various values of their lateral separation D measured as the distance between their middle lines in the undisturbed configuration of Fig. 1(1).

B. Computational Fluid Dynamics Solver

To resolve the fluid-solid interface of the undulating fish interacting with the fluid flow, a body-fitted approach is used in this paper which solves incompressible Navier-Stokes equations in the Arbitrary Eulerian Lagrangian formulation. It is spatially discretized with high-order spectral-element method (SEM) in staggered $P_N - P_{N-2}$ formulation [29, 30]. Pressure p and velocity $\mathbf{u}$ are solved iteratively [31] and are decoupled through a standard operator splitting approach stated as:

$$\frac{\beta_k \bar{\mathbf{u}}}{\delta t} - \frac{\mu}{\rho}\Delta\bar{\mathbf{u}} = -\sum_{j=1}^{k}\frac{\beta_{k-j}}{\delta t}\mathbf{u}^{n+1-j} - [(\mathbf{u}_i - \mathbf{w})\cdot\nabla\mathbf{u}_i]^{n+1} - \frac{\nabla p_i^{n+1}}{\rho}, \tag{3}$$

$$\Delta(p_{i+1}^{n+1} - p_i^{n+1}) = \nabla\cdot(\frac{\beta_k\bar{\mathbf{u}}}{\delta t}), \tag{4}$$

$$\mathbf{u}_{i+1}^{n+1} = \bar{\mathbf{u}} - \frac{\delta t}{\beta_k}\nabla\cdot(p_{i+1}^{n+1} - p_i^{n+1}). \tag{5}$$

Here, δt is the time step size, β_k is the backward differentiation coefficient of order k, $\mathbf{w}$ is the mesh velocity calculated algebraically from an a-priori specified moving pattern of the fish middle line from Eq. (2), n is the time step index. To solve for the convective term and the pressure implicitly, a sub-iteration loop (index i) is employed [31, 32] to repeat the splitting operators Eq. (3), (4), (5) by updating $\mathbf{u}_i^{n+1}$ and p_i^{n+1} until $\frac{|\mathbf{u}_{i+1}^{n+1}-\mathbf{u}_i^{n+1}|_2}{|\mathbf{u}_i^{n+1}|_2}$, and $\frac{|p_{i+1}^{n+1}-p_i^{n+1}|_2}{|p_i^{n+1}|_2}$ converge to a certain tolerance. The tolerance is set here to be 10^{-6} for velocity and 10^{-5} for pressure, while the convergence is typically achieved within three to five iterations. Sub-iteration also alleviates the Courant stability constraint, allowing one to use larger time step sizes [31, 32]. For an additional stabilization, an explicit modal filtering with the weight of 0.01 is applied to the last two modes of the polynomial approximation [33, 34].

C. Self-Propulsion

When the fish begins to execute an undulatory motion according to Eq. (2), it gains thrust and moves in the direction of the thrust force. In this paper, we consider only the forward motion for self-propulsion [22, 27], with the lateral motion being fixed and not affected by swimming. It corresponds to a case when the fish can adjust its muscles to leverage the fluid force around it, so it can maintain its straight heading direction. Such adaptation does not neglect any energy consumption, as the input power is associated with the adapted flipping force.

In a single fish case, a tuna like fish is placed in the middle of a 2D box with the dimensions of $12L \times 4L$, with an inlet boundary located at a distance L, and an outlet boundary at a distance $11L$, from the head of the fish, while the upper and lower boundaries employing symmetry boundary conditions are $2L$ away from its initial body middle line. To model the fish self-propulsion, we adjust the incoming fluid velocity at the inflow boundary rather than physically move the fish forward.

In a fish pair case, the settings are similar, but now the two fishes are separated by the distance D between their original middle lines. The domain, for each case considering a different value of the separation D, is thus extended in y direction to keep the vertical symmetric boundaries at a distance $2L$ away from each fish. Additionally, the fishes are propelled as a pair, corresponding to their combined thrust forces and combined masses, again, by adjusting the velocity of the incoming flow. We argue that, as in a single fish case, this setup implicitly considers the fishes self-adjustment, through the muscle power, which allows them to maintain their relative position to each other, which is accordingly reflected in their input power.

Swimming speed U^{n+1} at time $n+1$ is then determined by the total propelling force F_x^{n+1} acting on the fish surface in x direction from a fish swimming locomotion. Discretizing the Newton's second law with implicit Euler, the

self-propelling speed equation can be stated as

$$U^{n+1} = U^n + \frac{F_x^{n+1}}{m}\delta t, \tag{6}$$

where m is the mass of one fish, or the combined mass of a fish pair. The effect from the moment is neglected in the present work similar to [22]. The fluid environment is considered to be water so the density of both fluid and fish is considered to be $1000\,\mathrm{kg/m^3}$ and the dynamic viscosity μ is $1 \times 10^{-3}\,\mathrm{kg/(m \cdot s)}$. Implicit Eq. (6) is solved through a fixed point iteration with Aitken relaxation [31, 35, 36].

D. Optimization

1. Geometric Constraints

To consider the optimization problem for the swimming motion, we need to specify the constraints for the optimization parameters $\{c_1, c_2\}$ from Eq. (2), which are set to allow for physically realizable swimming motions as

$$C = \begin{cases} |c_1 + c_2| & \leq & 0.1L; \\ -\frac{c_1^2}{4c_2} & \leq & 0.1L; \\ c_2 & \leq & 0. \end{cases} \tag{7}$$

The constraints have the following physical interpretation [1, 2, 22, 37]:

- The maximum amplitude of the tail motion is set to be $0.1L$.
- The maximum amplitude of the body motion can not exceed $0.1L$.
- The tail is flapping down at the start-up time $t = 0$. The flapping up configuration represents a symmetry transformation of the current configuration and is omitted from the optimization problem due to redundancy.

2. Swimming Efficiency

In this paper, we consider two optimization cases, corresponding, accordingly, to a propulsive efficiency and an energy conversion efficiency. Propulsive efficiency is defined as

$$\eta_1(c_1, c_2, t_1) = \frac{\int_0^{t_1} \oint_{body} -\sigma \cdot n_x \cdot U \mathrm{d}x\,\mathrm{d}t}{\int_0^{t_1} \oint_{body} -\sigma \cdot n_y \cdot v \mathrm{d}x\,\mathrm{d}t}, \tag{8}$$

and the energy conversion efficiency is defined as

$$\eta_2(c_1, c_2, t_2) = \frac{\int_{t_2-T}^{t_2} \frac{1}{2} m U^2 \mathrm{d}t}{\int_{t_2-T}^{t_2} \oint_{body} -\sigma \cdot n_y \cdot v \mathrm{d}x\,\mathrm{d}t}. \tag{9}$$

Here $T = f^{-1} = 1$ s is the tail-beat period, σ is the total Cauchy stress tensor which includes viscous and pressure forces, $\mathbf{n} = \{n_x, n_y\}$ is the outer unit normal vector on the body surface, $v(x,t) = \partial\, y_m(x,t)/\partial\, t$ is the lateral surface velocity due to undulation, and $U(t)$ is the propulsive forward velocity. Swimming modes $\{c_1, c_2\}$ correspond to "black-box" optimization parameters and are not explicitly present in the cost function definition of Eq. (8), (9), but rather their influence on the value of the cost function is obtained via the CFD simulation.

Both t_1 and t_2 could be any values, but in the current optimization procedure, t_1 is chosen to be $6T$ and t_2 is chosen to be t_s, which is a time required for a fish to reach a steady-state swimming motion, and is case-dependent (different for any particular swimming mode $\{c_1, c_2\}$). The steady-state motion is defined as the state where the mean of the forward propulsive fish velocity U in every period of tail beating seizes changing from cycle to cycle.

Propulsive efficiency represents the ratio of the total energy gained from swimming versus the total energy input due to undulation when the fish starts to swim from rest. It shows how energy can be transferred efficiently to a pure kinetic energy, indicating a fast and cost-efficient swimming motion during the start up.

After certain number of periods of swimming, fish will reach its steady state, when its mean propulsive velocity in one period becomes unchanged. It means that the thrust from undulation compensates the fluid drag, and the kinetic energy of that fish is balanced. When the steady state is reached, the energy conversion efficiency shows the cost effectiveness of maintaining such a speed.

3. CMA-ES Optimizer

To find the maximum values of the two swimming efficiency coefficients η_1 and η_2 under constraints C from Eq. (7), a gradient-free optimization procedure based on a Co-variance Matrix Adaptation Evolution Strategy (CMA-ES) [3] approach is used to search for the best swimming modes from varying c_1 and c_2. The algorithm is based on the principles of biological evolution. A population is given initially as the input and three operations are defined to modify the population members: *recombination/crossover*, *mutation* and *selection*. New candidate solutions are sampled according to a multivariate normal distribution in the $\mathbf{R}^n$. Recombination amounts to providing a new mean value for the distribution. Mutation amounts to adding a random vector, a perturbation with zero mean. Pairwise dependencies between the variables in the distribution are represented by a covariance matrix. The covariance matrix adaptation is a method to update the covariance matrix of this distribution.

III. Results

A. Propulsive Efficiency Optimization

The single fish propulsive efficiency optimization problem of Eqs. (7) and (8) has been solved with the evolutionary algorithm CMA-ES [3] by 7 cycles of the optimization procedure when $t_1 = 6T$ is fixed. The number of samples (population size) is 6 due to the minimum requirement for two variables. The description of the optimization procedure is presented in Fig. 2 illustrating the samples distributions, problem constraints, and the optimization trend.

To judge the performance of the optimization procedure, we can define the convergence rate for the algorithm as

$$\epsilon = \left| \frac{\eta(c_1^{i+1}, c_2^{i+1}, t) - \eta(c_1^i, c_2^i, t)}{\eta(c_1^i, c_2^i, t)} \right| \cdot 100\%, \tag{10}$$

where the tuples $\{c_1^i, c_2^i\}$ are the mean values for distribution after the i^{th} cycle of the optimization procedure, t stands for $6T$ in the propulsive efficiency optimization. The performance of the optimization procedure for the propulsive efficiency optimization is presented in Fig. 3, showing fast convergence of the algorithm as the new suggested mean $\{c_1, c_2\}$ values are used for the swimming mode.

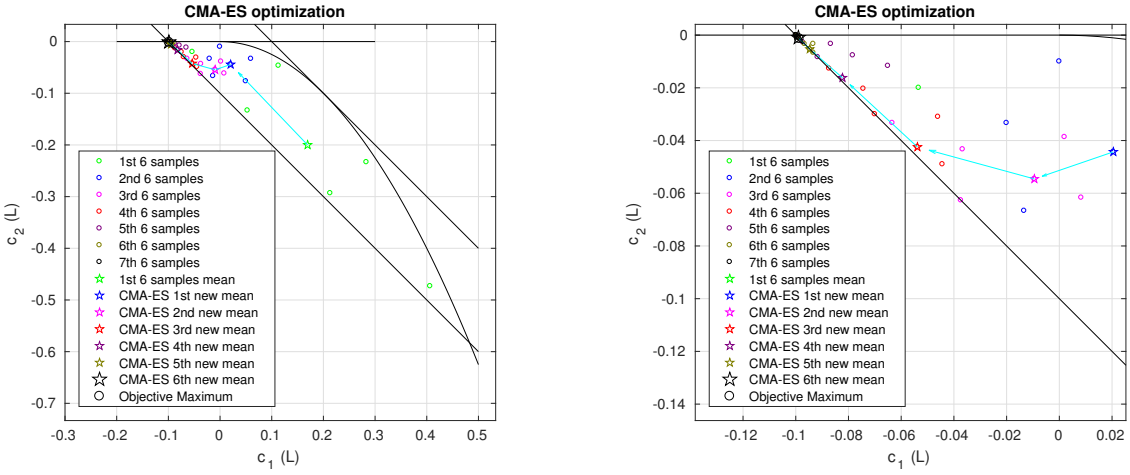

(a) Total cycles

(b) Last four cycles

Fig. 2 CMA-ES procedure for single fish propulsive efficiency.

The maximum efficiency converges to $\{c_1, c_2\} = \{-0.0987L, -0.0013L\}$ with a convergence rate of 0.4% and the maximum efficiency found is 0.1957 when $t_1 = 6T$. From the swimming mode $\{-0.0987L, -0.0013L\}$ (shown in Fig. 1(b)), one could tell that it reaches the maximum tail flipping and the quadratic part of the amplitude envelope is quite small. It shows that a brutal linear flapping might be the best way to have a high propulsive efficiency.

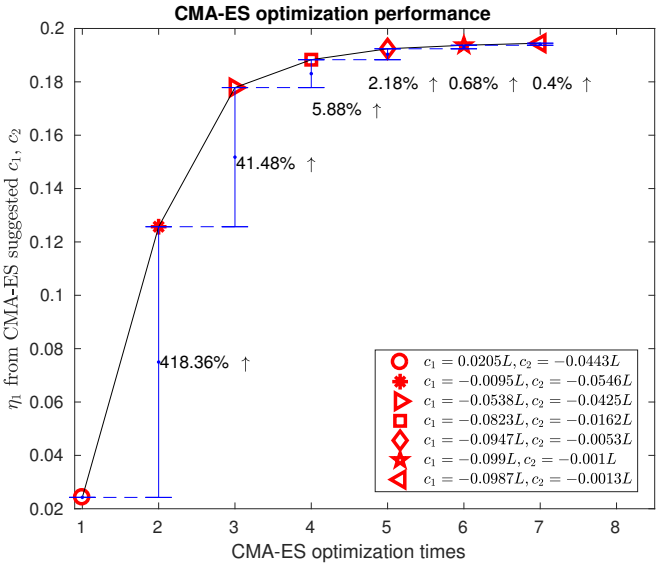

Fig. 3 Single fish propulsive efficiency optimization performance from consecutive suggested mean values for distribution. Values in % correspond to the convergence coefficient ϵ defined in Eq. (11).

B. Energy Conversion Efficiency Optimization

Similar to a propulsive efficiency optimization, energy conversion efficiency optimization problem of Eqs. (7), (9), is solved with 4 cycles and is shown in Fig. 4. The samples size is also 6 but $t_2 = t_s$, with the exact value varying depending on a particular swimming mode. The definition for the convergence rate is the same as in Eq. (11) albeit with $t = t_s$. The optimum efficiency after 4 cycles is found as $\eta_2 = 4.407$ when $\{c_1, c_2\} = \{0.0612L, -0.0273L\}$. Although the algorithm for the energy conversion efficiency optimization does not seem to converge as fast as for the propulsive efficiency optimization, visual inspection of the trend in the distribution samples from Fig. 4(a) shows that the optimum $\{c_1, c_2\}$ are confined to a significantly narrow region after 4 cycles. Different from the swimming mode $\{-0.0987L, -0.0013L\}$, optimum for a start-up motion, optimum mode $\{0.0612L, -0.0273L\}$ for a steady-state case shows more intense streamwise motion to reduce the fluid drag. One snapshot of these two optimum gaits is presented in Fig 1 (b).

C. Single Fish: Temporal Behavior of Swimming Efficiency

In the previous two optimization procedures, t_1 is chosen to be fixed as $6T$ and t_2 is equal to t_s to make sure fish is in its steady state. Here we compare how the two efficiency coefficients vary in time with several selected swimming modes $\{c_1, c_2\}$.

In Fig. 5, the two optimum gaits are highlighted and the rest are chosen for comparison. For the propulsive efficiency, the optimum propulsive swimming mode provides a fastest growth of efficiency versus time from the start-up. When t_1 becomes large enough and fish reaches its steady state, propulsive efficiency should decrease to 0 as no kinetic energy is gained while the input energy is still finite. It can be seen that for near-optimum propulsive efficiency modes showing faster growth, the maximum in time and the consecutive decrease is reached sooner, which means that for a fast start-up swimmer, its steady-state velocity is also reached sooner.

Different from propulsive efficiency, energy conversion efficiency in Fig. 5 (b) increases almost monothonically and stabilizes at its highest value, except for the mode that corresponds to an optimum propulsive efficiency η_1 of the optimization Case 1. This mode reaches a fairly high velocity that makes the flow increasingly turbulent, and the input energy increasingly variable from cycle to cycle. As a general observation, some swimming modes reach the steady state faster, while some need considerably longer time. However, the modes that reach the steady state faster are generally lower in energy conversion efficiency indicating that to maintain their speed at the steady state, it is not cost-efficient. The monothonically increasing trend shows that before the fish reaches its steady state, the cost effectiveness of energy conversion is always smaller than that in the steady state.

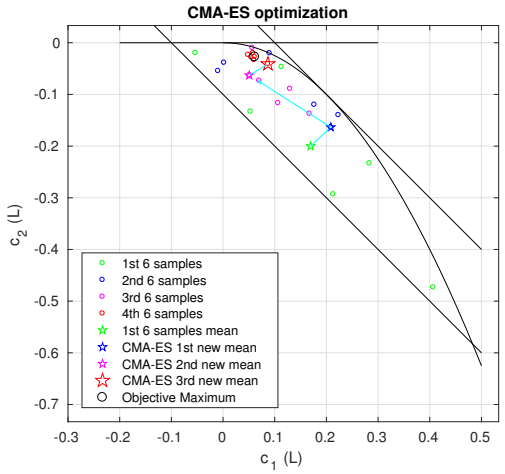

(a) Total cycles of CMA-ES procedure for single fish energy conversion efficiency.

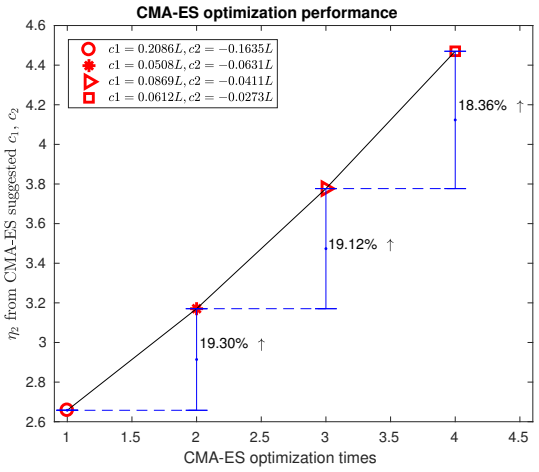

(b) Single fish energy conversion efficiency optimization performance from consecutive suggested mean values for distribution. Values in % correspond to the convergence coefficient ϵ defined in Eq. (11).

Fig. 4 CMA-ES procedure for single fish energy conversion efficiency.

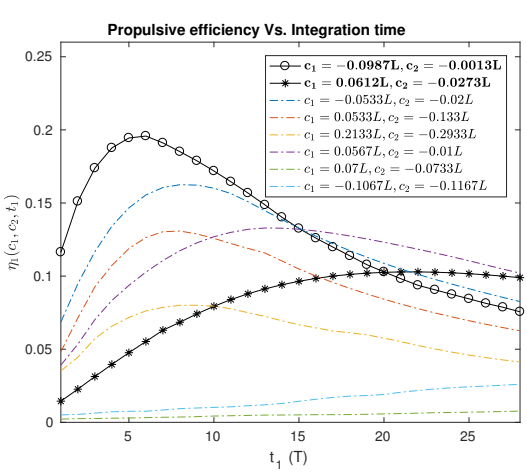

(a) Propulsive efficiency.

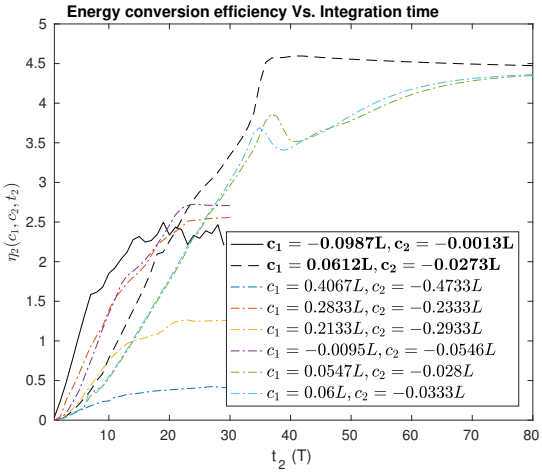

(b) Energy conversion efficiency.

Fig. 5 Change of efficiency coefficients for selected swimming modes with the integration time. Optimum modes for η_1, η_2 are highlighted in bold.

It is also reasonable to look into the relation between the steady-state forward mean velocity with the two efficiency coefficients. In Fig. 6, mean forward velocity in unit length L of one last period is compared with efficiency η_1 and η_2. It shows that η_1 has a positive correlation with the mean steady-state velocity. It indicates that if propulsive efficiency for $6T$ of a fish is large, then its steady-state velocity would be large as well. It assures a reasonable assumption that the swimming mode which is propulsive efficient is also fast swimming. As for energy conversion efficiency η_2, higher velocity mode tends to have a moderate efficiency while higher efficiency provides only a moderate or even low velocity. It is understandable, since if a fish is swimming in high speed, the input energy is also large due to a higher drag, which reduces the cost-efficiency. On the contrary, to maintain a relatively low speed is more cost-effective, since a lower fluid resistance needs to be overcome. Notice that there are few outliers in the plots, which show exceptionally low swimming speeds compared to the other modes at comparable efficiency, and their swimming modes are more likely not realistic or unnatural, although they are within the constraints.

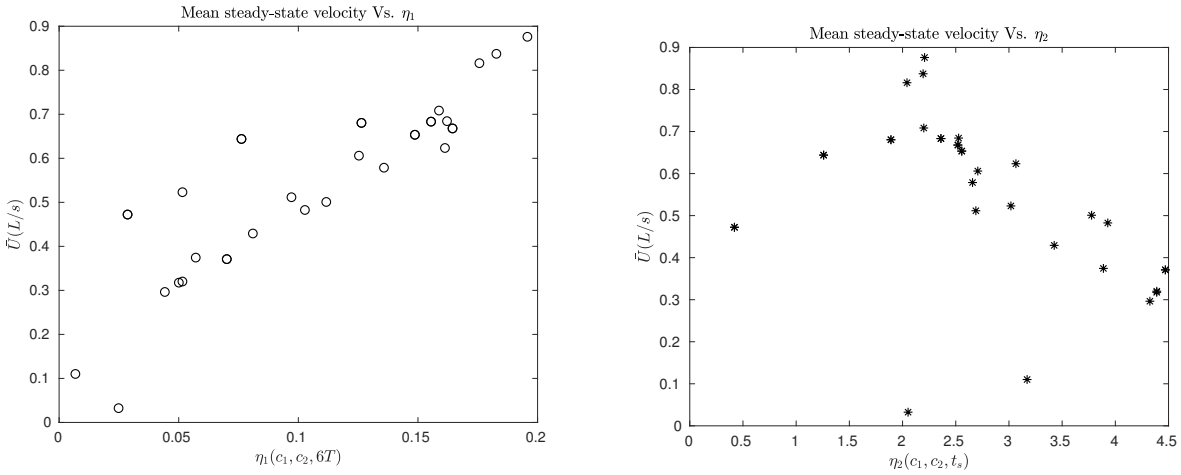

(a) Vs. Propulsive efficiency.

(b) Vs. Energy conversion efficiency.

Fig. 6 Mean steady-state swimming velocity in length L per second vs. different efficiency.

Another interesting comparison that can be done involves the correlation between the two efficiency coefficients. In Fig. 7, high energy conversion efficiency (η_2) mode tends to have a low propulsive efficiency (η_1), while a high propulsive efficiency (η_1) tends to have a moderate energy conversion efficiency (η_2). When energy conversion efficiency is high, its steady-state velocity is low, and in that sense, it is not high in propulsive efficiency. When a propulsive efficiency is high, it gives a high steady-state velocity which means a high kinetic energy, while it is also costly to maintain such a speed in terms of overcoming fluid resistance (drag), thus the energy conversion efficiency is moderate. Unfortunately, there is no perfect swimming mode that is high in both efficiency metrics, and thus, in reality, fish gaits would have to be adjusted to adapt to different circumstances.

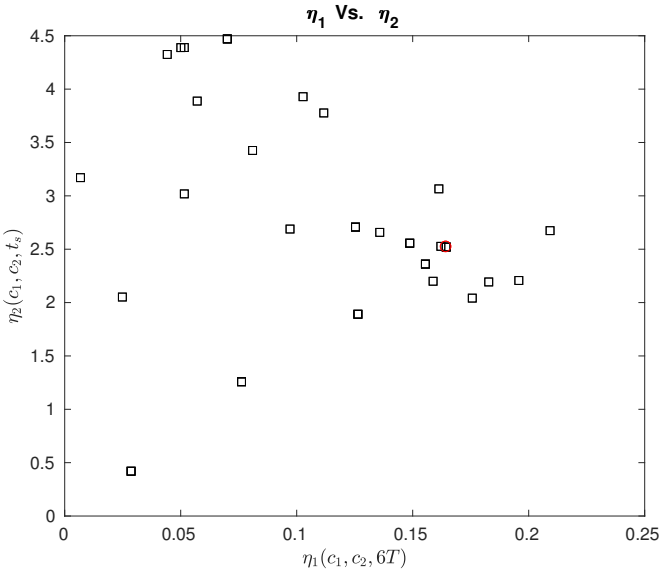

Fig. 7 Propulsive efficiency Vs. Energy conversion efficiency in various swimming modes. Mode selected later for a fish pair study is circled.

In Fig. 8, the vortex wakes for the two optimum swimming modes in terms of the propulsive efficiency, and the energy conversion efficiency, are presented. It can be noted that while the wake for the optimum propulsive efficiency shows a significant lateral undulation and high values of shed vorticity, consistent with a high tail amplitude motion of an

optimum start-up swimming mode, the wake for the optimum energy conversion efficiency mode is remarkably straight and the shed vorticity is weaker, corresponding to a more conservative undulatory motion and a more streamlined body position aimed at drag minimization.

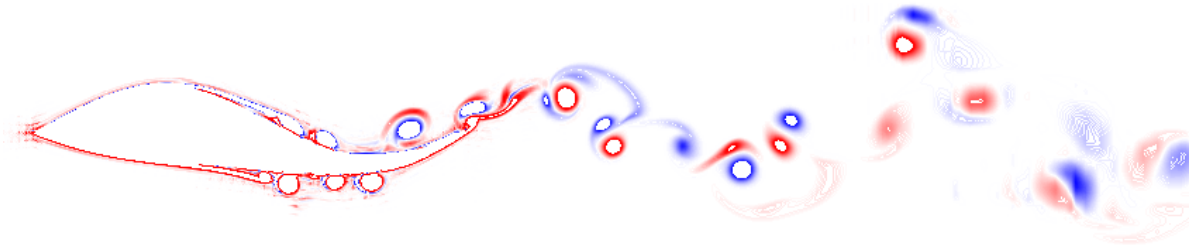

(a) Maximum propulsive efficient swimming mode.

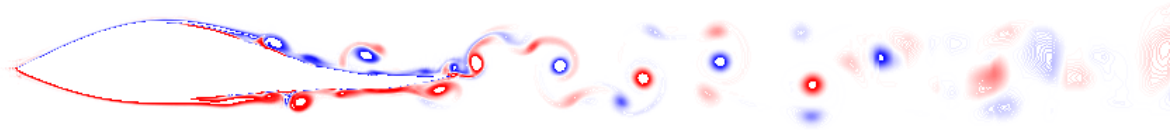

(b) Maximum energy conversion efficient swimming mode.

Fig. 8 Vortex wakes for fishes in different swimming mode. Red lines stand for positive vorticity, while blue lines stand for negative vorticity.

D. Pair Fish Swimming Efficiency

We now extend a single fish to a fish pair with various middle line distance separation values D of $0.67L$, L, and $1.33L$. A moderate swimming mode $\{c_1, c2\} = \{0.113L, -0.0467L\}$ corresponding to the values of $\{\eta_1, \eta_2\} = \{0.1645, 2.5201\}$ is selected for a general purpose of fish pair performance study. The selected swimming mode is circled in Fig. 7.

Two efficiency comparison with various integration time is shown in Fig. 9. When fish distance is increased to $D = 1.33L$, both anti-phase and in-phase results show a trend to match up the single fish results and almost no improvement or drawback could be seen as the fishes have a decreasing influence on each other when their separation is relatively large. However, for $D = 0.67L$, anti-phase swimming shows a strong improvement in propulsive efficiency while in-phase configuration shows a strong setback. As discussed previously, fast swimmers are not cost-effective, so it is reasonable for anti-phase motion to have a lower efficiency in energy conversion as observed.

For energy conversion efficiency, only in-phase swimming with $D = L$ shows higher efficiency than the single fish. To better look into the problem, Fig. 10 is presented with the fish pair mean steady-state velocity compared at different efficiencies. As can be told from the Figure, in-phase swimming with $D = L$ is slower than a single fish swimming which results in increase in the energy conversion efficiency. The speed of the in-phase swimming with $D = 0.67L$ is however too low, which, although decreases the fluid drag, also significantly lowers a kinetic energy, making the overall motion less energy-efficient.

From Fig. 10, anti-phase configuration provides better propulsive efficiency by reducing the input energy while keeping a similar value of the steady-state velocity. However, the in-phase configuration is shown to both reduce the efficiency of a stat-up motion and decrease the steady-state speed. However, this speed reduction seems to offer some in-phase configurations a relative small advantage with respect to the energy conversion efficiency. It is interesting to note, that, as compared to a single fish motion, a steady-state velocity is always reduced by all fish pair configurations at this particular swimming mode. The beneficial hydrodynamic interaction between the fishes can however result in a sufficiently lower input energy to reach its, although slightly lower, steady-state speed, which can increase the cost-effectiveness for both the start-up and the steady-state motion in fish arrays, however in different configurations.

The vortex wakes for the fish pair separated by the lateral distance $D = 0.67L$ for both anti-phase and in-phase configurations is shown in Fig. 11. As with a single fish motion, the anti-phase configuration that tends to be more efficient in start-up (higher propulsive effieciency) shows strongly undulating wakes, while in-phase configuration which is more drag-reducing and more energy efficient for a long-term swimming, shows significantly narrower wakes with a suppressed near-surface vorticity shedding.

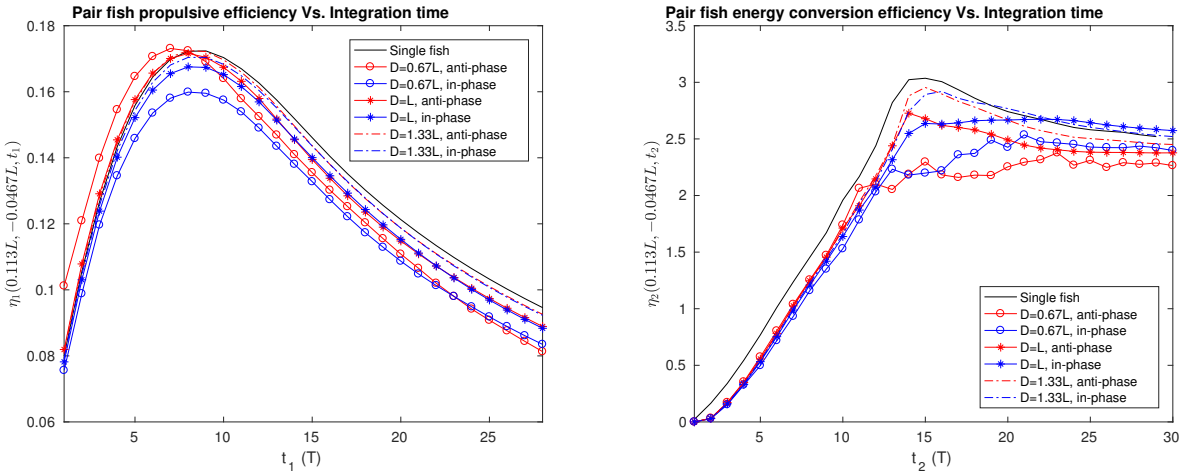

(a) Propulsive efficiency.

(b) Energy conversion efficiency.

Fig. 9 Efficiency comparison between different fish distances and phases for the same swimming mode.

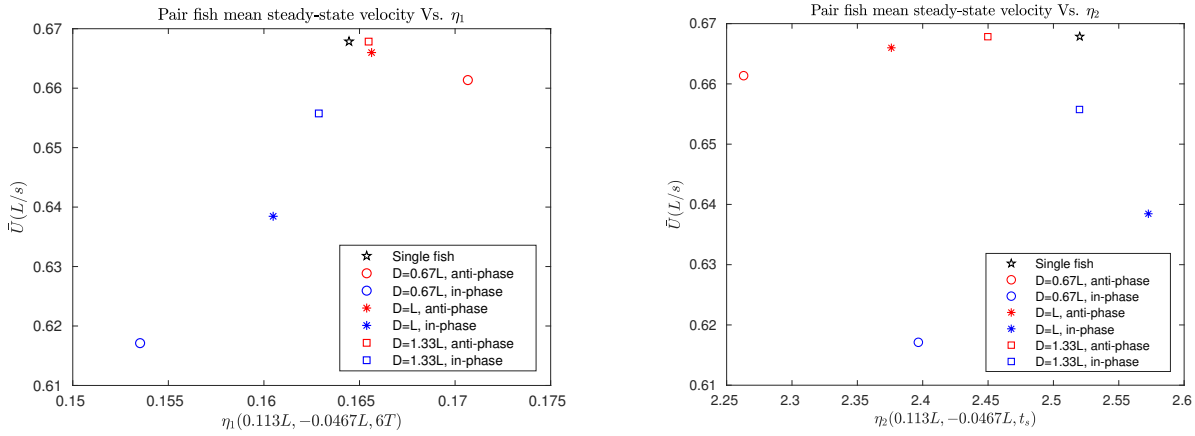

(a) Vs. Propulsive efficiency.

(b) Vs. Energy conversion efficiency.

Fig. 10 Mean steady-state swimming velocity for a fish pair in the units of length L per second vs. efficiency.

IV. Conclusion

In this paper, optimization of thunniform locomotion for a single fish propulsive efficiency and energy conversion efficiency, as well as the performance study of a fish pair has been considered. The computational framework has been developed that couples high-order fully resolved computational fluid dynamics simulations of flexible swimming bodies under water with a gradient-free optimization procedure based on evolution adaptation strategy. For a single swimmer, the optimum gaits of locomotion have been determined that maximize the propulsive efficiency and the energy conversion efficiency of undulatory motion with two optimization parameters. The relation between the two efficiency values and the swimming speed of the particular swimming modes has been discussed. For a fish pair, the separation

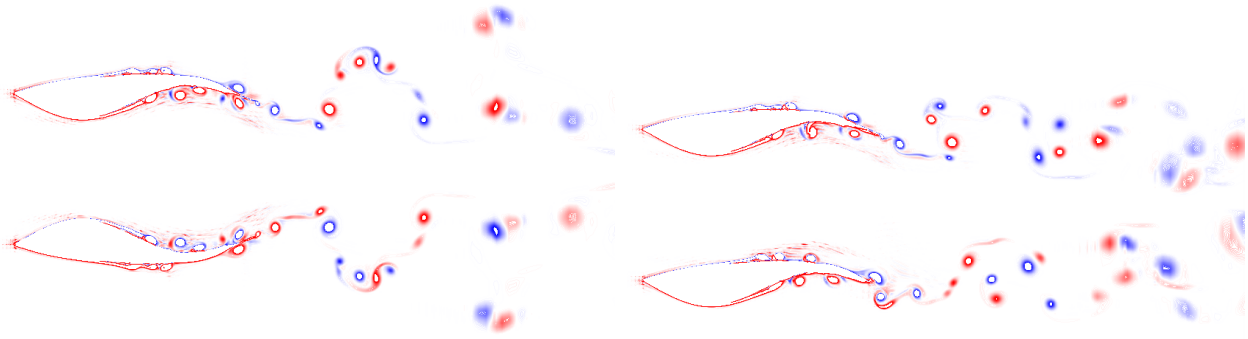

(a) Anti-phase. (b) In-phase.

Fig. 11 Vortex wakes for pair fish with distance 0.67L. Red lines stand for positive vorticity, while blue lines stand for negative vorticity.

distance between the fish has been shown to be influential for their swimming efficiency, with both the in-phase and the anti-phase undulatory synchronization between the swimmers. It was found that a swimming efficiency can be increased by a pair of fish as compared to a single fish, both for the propulsive efficiency, and the energy conversion efficiency, albeit by different fish pair configurations. The vortex wakes for the two optimum modes of motion (propulsion efficient versus energy efficient) have been compared and analyzed both for a single fish and a fish pair.

References

[1] y Alvarado, P. V., "Design of Biomimetic Compliant Devices for Locomotion in Liquid Environments," Ph.D. thesis, Massachusetts Institute of Technology, Cambridge, Feb. 2007.

[2] y Alvarado, P. V., and Youcef-Toumi, K., "Soft-Body Robot Fish," *Robot Fish Bio-inspired Fishlike Underwater Robots*, Springer, 2015, pp. 161–191.

[3] Hansen, N., and Ostermeier, A., "Completely derandomized self-adaptation in evolution strategies," *Evolut. Comp.*, Vol. 9, No. 2, 2001, pp. 159–195.

[4] Weihs, D., "Hydrodynamics of fish schooling," *Nature*, Vol. 241, 1973, pp. 290–291.

[5] Shaw, E., "Schooling fishes," *Am. Sci.*, Vol. 66, 1978, pp. 166–175.

[6] Barnes, R. S. K., and Hughes, R. N., *An Introduction to Marine Ecology*, Blackwell, 1988.

[7] Pitcher, T. J., Magurran, A. E., and Winfield, I. J., "Fish in larger shoals find food faster," *Behav. Ecol. Sociobiol.*, Vol. 10, 1982, pp. 149–151.

[8] Partridge, B. L., and Pitcher, T. J., "Evidence against a hydrodynamic function for fish schools," *Nature*, Vol. 279, 1979, pp. 418–419.

[9] Major, P. F., "Predator-prey interactions in two schooling fishes, *Caranx ignobilis* and *Stolephorus purpureus*," *Animal Behaviour*, Vol. 26, 1978, pp. 760–777.

[10] Aoki, I., "A simulation study on the schooling mechanism in fish," *Bull. Japan. Soc. Sci. Fisheries*, Vol. 48, 1982, pp. 1081–1088.

[11] Couzin, I. D., Krause, J., James, R., Ruxton, G. D., and Franks, N. R., "Collective Memory and Spatial Sorting in Animal Groups," *J. Theor. Biol.*, Vol. 218, 2002, pp. 1–11.

[12] Shaukat, M., and Chitre, M., "Bio-inspired Practicalities: Collective Behaviour using Passive Neighbourhood Sensing," *Proceedings of the 14th International Conference on Autonomous Agents and Multiagent Systems (AAMAS 2015)*, 2015. Bordini, Elkind, Weiss, Yolum (eds.), May 4–8, 2015, Istanbul, Turkey.

[13] Couzin, I. D., Krause, J., Franks, N. R., and Levin, S. A., "Effective leadership and decision making in animal groups on the move," *Nature*, Vol. 433, 2005, pp. 1–11.

[14] Hemelrijk, C. K., and Hildenbrandt, H., "Schools of fish and flocks of birds: their shape and internal structure by self-organization," *Interface Focus*, Vol. 2, 2012, pp. 726–737.

[15] Huntley, M. E., and Zhou, M., "Influence of animals on turbulence in the sea," *Mar. Ecol. Prog. Ser.*, Vol. 273, 2004, pp. 65–79.

[16] Fukuda, H., Torisawa, S., Sawada, Y., and Takagi, T., "Ontogenetic changes in schooling behaviour during larval and early juvenile stages of pacific bluefin tuna thunnus orientalis," *J. Fish Biol.*, Vol. 76, 2010, pp. 1841–1847.

[17] Zuyev, G. V., and Belyaev, V. V., "An experimental study of the swimming of fish in groups as exemplified by the horsemackerel," *J. Ichthyology*, Vol. 10, 1970, pp. 545–549.

[18] Marras, S., Killen, S. S., Lindström, J., McKenzie, D. J., Steffensen, J. F., and Domenici, P., "Fish swimming in schools save energy regardless of their spatial position," *Behav. Ecol. Sociobiol.*, Vol. 69, 2015, pp. 219–226.

[19] Tsang, A. C. H., and Kanso, E., "Dipole interactions in doubly periodic domains," *J. Nonlinear Sci.*, Vol. 23, 2013, pp. 971–991.

[20] Gazzola, M., Tchieu, A. A., Alexeev, D., de Brauer, A., and Koumoutsakos, P., "Learning to school in the presence of hydrodynamic interactions," *J. Fluid Mech.*, Vol. 789, 2016, pp. 726–749.

[21] Shirgaonkar, A. A., MacIver, M. A., and Patankar, N. A., "A new mathematical formulation and fast algorithm for fully resolved simulation of self-propulsion," *J. Comp. Phys.*, Vol. 228, 2009, pp. 2366–2390.

[22] Borazjani, I., and Sotiropoulos, F., "On the role of the form and kinematics of self-propelled body/caudal fin swimming," *J. Exper. Biology*, Vol. 213, 2010, pp. 89–107.

[23] Xu, Y.-G., and Wan, D.-C., "Numerical simulation of fish swimming with rigid pectoral fins," *J. Hydrodynamics*, Vol. 24, No. 2, 2012, pp. 263–272.

[24] Kern, S., and Koumoutsakos, P., "Simulations of optimized anguilliform swimming," *J. Exp. Biol.*, Vol. 209, 2006, pp. 4841–4857.

[25] van Rees, W. M., Gazzola, M., and Koumoutsakos, P., "Optimal morphokinematics for undulatory swimmers at intermediate Reynolds numbers," *J. Fluid Mech.*, Vol. 775, 2015, pp. 178–188.

[26] Eloy, C., "On the best design for undulatory swimming," *J. Fluid Mech.*, Vol. 717, 2013, pp. 48–89.

[27] Bergmann, M., and Iollo, A., "Modeling and simulation of fish-like swimming," *J. Comp. Phys.*, Vol. 230, 2011, pp. 329–348.

[28] Zhu, Q., Wolfgang, M. J., Yue, D. K. P., and Triantafyllou, M. S., "Three-dimensional flow structures and vorticity control in fish-like swimming," *J. Fluid Mech.*, Vol. 468, 2002, pp. 1–28.

[29] Deville, M. O., Fischer, P. F., and Mund, E. H., *High-order methods for incompressible fluid flow*, Cambridge University Press, Cambridge, UK, 2002.

[30] Fischer, P., "An Overlapping Schwarz Method for Spectral Element Solution of the Incompressible Navier-Stokes Equations," *J. Comp. Phys.*, Vol. 133, 1997, pp. 84–101.

[31] Xu, Y., and Peet, Y. T., "Accuracy and performance of fluid-structure interaction algorithms with explicit versus implicit formulations of the fluid solver," AIAA Paper 3449, 2017. In 3rd AIAA Computational Fluid Dynamics Conference/AIAA Aviation Forum and Exposition, Denver, CO, June 2017.

[32] Baek, H., and Karniadakis, G. E., "Sub-iteration leads to accuracy and stability enhancements of semi-implicit schemes for the Navier-Stokes equations," *Journal of Computational Physics*, Vol. 230, 2011, pp. 4384–4402.

[33] Fischer, P., and Mullen, J., "Filter-based stabilization of spectral element methods," *C. R. Acad. Sci. Paris*, Vol. 332, 2001, pp. 265–270.

[34] Chatterjee, T., and Peet, Y. T., "Regularization modelling for large-eddy simulation in wall bounded turbulence: an explicit filtering-based approach," *Int. Journal Numer. Methods Fluids*, 2018, pp. 1–17. DOI: 10.1002/d.4508.

[35] Irons, B. M., and Tuck, R. C., "A version of the Aitken accelerator for computer iteration," *International Journal for Numerical Methods in Engineering*, Vol. 1(3), 1969, pp. 275–277.

[36] Küttler, U., and Wall, W., "Fixed-point fluid-structure interaction solvers with dynamic relaxation," *Computational Mechanics*, Vol. 33, 2004, pp. 839–848.

[37] Hultmark, M., Leftwich, M., and Smits, A. J., "Flowfield measurements in the wake of a robotic lamprey," *Exp. Fluids*, Vol. 43, 2007, pp. 683–690.